DNP-Supported Solid-State NMR Studies of 13C,15N,29Si-Enriched Biosilica of Cyclotella Cryptica and Thalassiosira Pseudonana

Helena Ehren
Universiteit Utrecht
Felicitas Kolbe
Technische Universitat Dresden
Alesandra Lucini Paioni
Universiteit Utrecht
Eike Brunner
Technische Universitat Dresden
Marc Baldus (m.baldus@uu.nl)
Universiteit Utrecht https://orcid.org/0000-0001-7068-5613

Research article

Keywords: Solid-state NMR spectroscopy, DNP, diatoms, Cyclotella cryptica, Thalassiosira pseudonana, Chitin, LCPAs

Posted Date: July 23rd, 2020

DOI: https://doi.org/10.21203/rs.3.rs-44217/v1

Version of Record: A version of this preprint was published at Discover Materials on March 29th, 2021.
See the published version at https://doi.org/10.1007/s43939-021-00009-9.

Abstract

Solid-state NMR spectroscopy represents a powerful method for the investigation of diatom biosilica but detailed studies regarding its chemical composition and structural organization can be prohibited by insufficient spectroscopic sensitivity. Here, we used two-dimensional (2D) Dynamic Nuclear Polarization (DNP)-supported solid-state NMR experiments to obtain information about the molecular composition and supramolecular organization of proteins and carbohydrates in ^{13}C,^{15}N,^{29}Si-labeled biosilica of *C. cryptica.* As a reference, we conducted DNP experiments on isotope-labeled biosilica of *T. pseudonana*. DNP-enhancement factors for different NMR signals, and thus, for different organic compounds, provide information about the supramolecular architecture of the biosilica. In addition, DNP-supported heteronuclear nitrogen-carbon correlation experiments allowed us to prove the presence of different LCPAs (long chain polyamines) and revealed the occurrence of amine-nitrogen moieties exhibiting a correlation with carbonyl carbons that may indicate cross-linking of LCPAs to proteins as previously seen in studies on proteins extracted from other diatoms.

Introduction

Solid-state NMR spectroscopy is a powerful method for the investigation of biomaterials[1–7] including diatom biosilica[8]. Diatoms are unicellular algae. They are frequently studied model organisms for biomineralization research and also of significant interest in the context of designing bioinspired materials[3, 8–11]. The silica phase of the cell walls can be characterized using ^{29}Si solid-state NMR spectroscopy and the organic compounds by ^{13}C and ^{15}N solid-state NMR spectroscopy[3, 8–11]. The sensitivity of such experiments is strongly enhanced by isotope-labeling which, as shown by Brunner et al.[8] can be elegantly achieved by diatom growth in isotope-enriched culture medium. In recent years, high-frequency Dynamic Nuclear Polarization[12] (DNP), in which polarization is transferred from free electrons to atomic nuclei has become a powerful method to enhance solid-state NMR signal intensities by up to two orders of magnitude. These advancements have greatly expanded the use of ssNMR to study complex biomolecular systems including membrane[13–18] and amyloid[19–20] proteins as well as cellular preparations[21–24] and biomaterials[2–4, 25]. Such experiments not only enhance the prospects to study local molecular structure but also offer a spectroscopic means to probe local as well as supramolecular arrangements[19] as we have previously shown for diatom biosilica from *Stephanopyxis turris*[3].

In the present work, we have used DNP-ssNMR to examine isotope-labeled diatoms of *Cyclotella cryptica* biosilica[26]. In particular, the use of DNP allowed us to study the presence of silica-attached chitin. In addition, we could spectroscopically probe LCPAs and we examined the organic-inorganic interface in *C. cryptica.* We compare our findings to experimental results obtained on *Thalassiosira pseudonana* and our previously published results on *S. turris* biosilica[3].

Methods

DNP sample preparation of ^{13}C,^{15}N,^{29}Si-enriched and ^{13}C-enriched C. cryptica & T. pseudonana biosilica

Cultivation of both diatom species *C. cryptica* and *T.pseudonana* was performed in sealed 20 L plastic containers in an artificial seawater (ASW) corresponding to a recipe of the North East Pacific Culture Collection[27]. For isotope-labeling the enriched salts $NaH^{13}CO_3$ (Sigma Aldrich, 98 at.%), $Na^{15}NO_3$ (Sigma Aldrich, 98 at.%) and $Na_2{}^{29}SiO_3$ were added. ^{29}Si-enriched $Na_2{}^{29}SiO_3$ was prepared using a well-established protocol for a solid phase reaction of $^{29}SiO_2$ (CortecNet, 99.9 at.%) and Na_2CO_3 (Grüssing).[10, 28] Growth conditions were set to a temperature of 18 °C and a day/night-lighting cycle of 12 h/12 h. The pH was set to 8.0–8.2. The cells were harvested by centrifugation. The cell pellet was cleaned using a lysis buffer solution containing 0.1 M EDTA (ethylenediaminetetraacetic acid, isocommerz) and 2 wt-% SDS (sodium dodecyl sulfate, Merck KGaA) at pH 8.0. The suspension was heated to 95 °C for 10 min. Then the cells were centrifuged (2870 *g*, 10 min) and the supernatant was decanted. The cells were resuspended in new lysis buffer solution and the procedure was repeated up to 5 times, until the supernatant was nearly colorless and the cell walls were nearly white. The sample was washed three times with ultrapure water and freeze-dried.

DNP-supported NMR experiments

1. NMR sample preparation using the incipient wetness method

3.2 mm sapphire rotors were filled with isotope-labeled *C. cryptica or T. pseudonana* biosilica which were wetted directly before measurements. The wetting of the biosilica was performed using the method of incipient wetness impregnation with the radical solution at room temperature.[21] The radical stock solution with a concentration of 15 mM was prepared by dissolving AMUPol in D_2O/H_2O 9:1. The solution was stored at -20 °C. 10.2 mg of biosilica were wetted with 50 µL AMUPol solution. Directly afterwards, the filled rotors were transferred to the NMR probe which was cooled to 92 K.

2. DNP-supported NMR experiments

DNP experiments were acquired using a ^{1}H-^{13}C-^{15}N triple resonance probe at a static magnetic field of 9.4 T corresponding to proton/electron resonance frequencies of 400 MHz/ 263 GHz (Bruker BioSpin). The temperature was set to 100 K and the spinning speed to 9 kHz. The SPINAL-64 sequence[29] was used for proton decoupling at 85 kHz. The recycle delay was set to 2 s for all experiments. For 2D proton-driven spin diffusion (PDSD) experiments, Carbon-carbon mixing was established with a mixing time of 50 ms and the H-C CP contact time was set to 700µs. For the isotope-enriched *C. cryptica* biosilica sample, 224 scans were acquired with acquisition times of 15 ms and 6 ms for the direct and indirect dimensions, respectively. For the isotope-enriched *T. pseudonana* biosilica sample, 64 scans were acquired with acquisition times of 15 ms and 7 ms for the direct and indirect dimensions, respectively. In both cases two spectra were recorded, with and without DNP, and 1D slices were used to calculate the DNP enhancement. The ^{15}N -^{13}C correlation experiment was performed using a H-N CP step of 1 ms and a

SPECIFIC-CP transfer step of 2.5 ms. Acquisition times were 8 ms and 7.5 ms for the direct and indirect dimensions, respectively. 256 scans were acquired and the spectrum was processed using a 0.5 π shifted sine squared window function in both dimensions The ^{15}N-edited PDSD experiment[30] was recorded using a SPECIFIC-CP transfer step of 2.5 ms which is typical for one-bond NC correlations experiments[31] and a carbon-carbon mixing time of 50 ms. 1728 scans were acquired with acquisition times of 10 ms and 4 ms for the direct and indirect dimensions, respectively. The center frequencies were set to 50 ppm for ^{15}N and ^{13}C dimensions. The spectrum was processed using a 0.33 π shifted sine squared window function in both dimensions.

Results And Discussion

In our previous study[26] of *C. cryptica* using conventional 1D and 2D ssNMR spectroscopy, we observed that a high amount of proteins is associated to the biosilica and we detected two different chitin conformations. In the following, we used DNP-supported NMR experiments to further enhance ssNMR signal intensities. As mentioned above, DNP relies on spin polarization transfer from electron spins to nuclei. In our experiments, samples were impregnated with a “DNP juice” (see methods) containing the biradical AMUPol[32]. First, we conducted one-dimensional ^{13}C and ^{15}N detected CP experiments (Fig. 1) under DNP conditions and, as in our previous study[3], defined the DNP enhancement factor by the ratio of signal intensities with and without microwave irradiation. In ^{13}C CP experiments, we observed enhancement factors that (except for carbohydrates) ranged between 18 and 26 (Fig. 1, left). In the ^{15}N CP measurement, we observed an enhancement of 26 for both amide and amine ^{15}N signals (Fig. 1, right). As we have discussed elsewhere[26], *C. cryptica* contains a massive organic matrix and produces extracellular chitin fibrils of ca. 50 nm thickness[33–34] (see also Figure S1).

To further investigate molecule-specific DNP enhancements, we performed a two-dimensional DNP-enhanced PDSD (Proton-Driven Spin Diffusion) experiment (Fig. 2). We observed similar ^{13}C-^{13}C correlations as in the standard PDSD experiment[26], however with considerably higher signal intensities. This enabled the detection of new signals which are not observable in the conventional experiment. In particular, two spin systems with several correlations are observable: One spin system shows correlations from 92 ppm to 81 ppm, 75 ppm, and 72 ppm. The other system shows correlations from 95 ppm to 81 ppm, 75 ppm, 73 ppm, and 70 ppm. (Fig. 2, framed in blue). These correlations are characteristic for carbohydrates, where the C1 is not connected. These unconnected anomeric carbon atoms characteristically give rise to peaks between 90 and 100 ppm. In this case both spin systems also contain a shift higher than 80 which indicates a substitution on the carbocycle[35] by e.g. another sugar. This points towards the presence of reducing ends of polysaccharides[36]. A monosaccharide analysis which provides information about the total carbohydrate composition revealed glucose and mannose as main monosaccharides. Xylose, ribose, fucose, galactose and glucosamine are also present in significant concentrations[26]. However, a differentiation between monosaccharides and monosaccharide units from polysaccharides is not possible due to the performed hydrolysis step.

Moreover, the determination of DNP enhancement factors for different signals, which are characteristic for different organic compounds, can help to probe the supramolecular architecture of the biosilica[3]. To distinguish DNP enhancements of protein and carbohydrate signals, we analyzed different 1D slices of the 2D spin diffusion experiment (Fig. 2). For the protein signals, we examined a 1D slice at 53 ppm which is typical for protein backbone Cα resonances and observed a strong enhancement factor of 26 in line with our 1D ^{15}N CP signals (Fig. 1). Thus, the proteins should be located at the solvent-accessible surface of the biosilica, where the radical solution (AMUPol) can polarize nuclei located in the biomolecules. In contrast, for the carbohydrate region, e.g. the signals at 105 ppm, we determined significantly lower enhancement factors between 5–8 which is close to the ^{13}C enhancements seen in 1D CP MAS for carbohydrates (Fig. 1). Note that in the latter case, a precise determination of the DNP enhancements for carbohydrates may be complicated due to the overlapping MAS sidebands from other carbon species.

As discussed elsewhere[3, 19, 37], the DNP enhancement in complex biomolecules depends on the internuclear distances between hydrogens responsible for the polarization transfer via proton-driven spin diffusion and the macromolecular layer size. In addition, the DNP enhancement for biomolecules close to the radical, may itself be modulated by the details of the local electron-nucleus geometry. This geometry determines the spin-diffusion barrier[38], influences the DNP magnetic field dependence of the DNP effect[39] and leads to paramagnetic line broadening[14, 40] within a sphere of about 1 nm around the DNP radical[14]. We expect this effect to be particularly strong for biosilica such as from *S. turris* which are characterized by small protein/organic surface layers[3]. Indeed, DNP signal enhancements for polyssacharides and polyamines amounted to about 40% to the protein signal enhancements for *S. turris*[3]. In contrast, the organic layer for *C. cryptica* is significantly larger[26] which results in almost uniform DNP enhancements in 1D ^{13}C CP MAS data and is possibly the reason for the larger (relative) decrease in DNP enhancement from 26 to 5–8 for carbohydrates.

Note that the increased line broadening often observed at low-temperature DNP conditions[14] prevents the differentiation between the α-like chitin- and β-chitin signals as it was possible without DNP and at ambient sample temperatures[26]. On the other hand and as mentioned earlier, *C. cryptica* contains a massive organic matrix and produces extracellular chitin fibrils of ca. 50 nm thickness[33–34]. Hence, a more detailed analysis employing a classical spin-diffusion approximation to correlate relative DNP enhancements with biosilica layer thickness as done earlier for labeled diatom biosilica of *S. turris* [3] was not attempted here. Instead we can draw the following general conclusions. Firstly, we would expect from previous theoretical work from our laboratory[37] only minor changes for the DNP enhancement for chitin embedded in the extracellular chitin fibrils compared to the protein layer. On the other hand, fluorescence spectroscopy[41] has shown that chitin in *C. cryptica* biosilica can also be directly associated to the siliceous cell walls. For this species, that is potential surrounded by low density of hydrogens that limit the spin-diffusion process, low DNP enhancements as found in Fig. 2 may be possible. Since ssNMR

detects the entire ensembles of chitin moieties in our sample, the latter species may hence represent a prominent fraction in our *C. cryptica* preparations.

To further investigate the carbohydrate association to the siliceous cell walls, we conducted similar experiments on isotope-enriched *T. pseudonana* biosilica (Fig. 3) for which the presence of a chitin-based meshwork is already known[11]. Again, we analyzed 1D slices typical for protein and carbohydrate signals and observed a strong enhancement factor of 32 for the protein Cα signals (signal at 53 ppm). In line with our earlier observations, the proteins are thus predominately located at the solvent-accessible surface of the biosilica, where the radical solution (AMUPol) can polarize nuclei located in the biomolecules. Remarkably, for the carbohydrate region, e.g. the signals resonating at 105 ppm, a lower enhancement compared to the protein signals is again observed. However, the relative enhancement of about 15 is significantly larger than in the case of *C. cryptica* biosilica (amounting to 5–8). These findings would be consistent with the notion that the organic matrix of *T. pseudonana* biosilica is less pronounced than in the case of *C. cryptica* [26] but larger than for *S. turris.* Such an interpretation would be consistent with previous findings[42].

Moreover, our DNP experiments revealed the presence of additional carbohydrate species as seen before for *C. cryptica* (Fig. 2). Interestingly, one of the observed new sugar spinsystems exhibits a correlation of the anomeric carbon to a signal around 165 ppm (Figure S2). Sp^2-configured carbon atoms of nitrogen containing functional groups including imines[43] and guanidiniums[44] as well as amide carbonyls give rise to peaks in this region. This correlation could hence indicate a cross linking between a carbohydrate C1 and an amino acid such as the guanidinium containing arginine, which has rarely been described as part of *N*-glycans. Another possibility would be the presence of citrulline as its carboxamide gives rise to resonances at around 164 ppm and it has been described as being linked to polysaccharides before[45]. This link could represent the interface of the sugarlayers with the residual organic matrix.

Finally, we used DNP-supported ^{15}N-^{13}C correlation experiments to further investigate proteins as well as the presence of LCPA in our preparations. Again, DNP greatly facilitated such experiments because of the increased spectroscopic sensitivity, thereby reducing measurement times. To study nitrogen containing ^{13}C moieties, we performed ^{15}N filtered experiments[30–31]. Figure 4 (red spectrum) shows an ^{15}N-^{13}C correlation spectrum where magnetization is first transferred from ^{1}H to the ^{15}N labelled amines of the LCPAs followed by a ^{15}N-^{13}C CP transfer to nearby ^{13}C carbons (typically separated by one chemical bond in fully labelled proteins[31]). The introduction of a spin diffusion (mixing) step between carbons allowed us to study more distant ^{13}C atoms including polyamines (blue spectrum). Figure 4 shows the ^{15}N-^{13}C correlations of the LCPA region, exclusively. The former discussed NMR spectra show the presence of LCPAs within the biosilica sample. Carbon signals between 30–70 ppm correlate with nitrogen signals between 30–60 ppm. Signals between 20–60 ppm in the nitrogen dimension correspond to the primary, secondary and tertiary amines of LCPAs as well as lysine side chains. These correlate with carbon signals between 45–70 ppm characteristic for carbon atoms that are connected to amines. Due to the expected manifold of LCPAs in the sample, we detected various intense correlation signals. In the NCC

experiment with a mixing time of 50 ms, correlations between carbon atoms with longer distances to the amine-nitrogen can be observed. Thus, an increasing number of correlations occurs, e.g., correlations to alkyl groups at lower ^{13}C chemical shift between 15–30 ppm. Interestingly, we even observed a correlation to carbonyl-carbons at 174 ppm. This signal occurs probably due to relay transfer between close-by ^{13}C labeled atoms to a carbonyl atom as usually seen in fully labeled protein samples under MAS conditions (see e.g. Ref.[46]) Such a correlation between the amine of a LCPA and a carbonyl group was not observed for other diatom biosilica, including diatom biosilica from *S. turris*[3]. However, it is well known from the model organism *T. pseudonana*[11] that LCPAs can be covalently attached to lysine residues or posttranslational modified hydroxylysine residues that may give rise to the correlation seen at 174 ppm. Additionally, the chemical shift of this carbonyl group is more typical for carbonyl groups of proteins. The above discussed chitin should give rise to a signal at a higher chemical shift of ca. 176 ppm. Thus, proximity between amine nitrogens and protein carbonyl groups is more likely here.

Conclusions

Our DNP-supported solid-state NMR studies provide further insight into the composition and architecture of *C. cryptica* biosilica and allow to draw the following conclusions:

1. We could confirm the presence of chitin seen in ssNMR conducted at ambient temperatures[26] using PDSD experiments performed under DNP conditions. The calculated enhancement factors reveal changing DNP enhancements for different types of biomolecules. The enhancement factor of 26 for proteins is clearly higher than the values of 5–8 for carbohydrates. This result shows that the accessibility of proteins in contrast to carbohydrates is in qualitative agreement with previous DNP-studies of biosilica from the species *S. turris*.[16]
2. We also observed a reduced DNP efficiency for carbohydrates compared to protein signals in preparations of *T. pseudonana* biosilica. However, this reduction was lower than for the case of *C. cryptica* biosilica. Together with our previous results on *S.turris* we attribute these variations to an increasing size of organic layers towards *C. cryptica* biosilica where paramagnetic quenching due to the presence or binding of DNP radicals has the smallest influence on the observed protein signal under DNP conditions.
3. DNP-supported ^{15}N-^{13}C 2D correlation experiments prove the presence of different LCPAs. Interestingly, a correlation of amine-nitrogen to a carbonyl carbon can be observed which may reflect chemical linkage to proteins as previously seen in studies on *T. pseudonana* [47–48].

<

Abbreviations

2D two-dimensional

AMUPol 15-{[(7-oxyl-3,11-dioxa-7-azadispiro[5.1.5.3]hexadec-15-yl)carbamoyl][2-(2,5,8,11-tetraoxatridecan-13-ylamino)}-[3,11-dioxa-7- azadispiro[5.1.5.3]hexadec-7-yl])oxidanyl

ASW artificial seawater

C. cryptica Cyclotella cryptica

CP cross polarization

DNP Dynamic Nuclear Polarization

EDTA ethylenediaminetetraacetic acid

LCPA long-chain polyamine

MAS magic angle spinning

NC ^{15}N-^{13}C correlation spectrum

NCC ^{15}N-^{13}C –^{13}C correlation spectrum

NMR nuclear magnetic resonance

PDSD proton-driven spin-diffusion

ppm parts per million

SPECIFIC-CP Spectrally induced filtering in combination with cross polarization

RF radio frequency

SPINAL64 small phase incremental alternation, with 64 steps

ssNMR solid-state NMR

S. turris Stephanopyxis turris

T. pseudonana Thalassiosira pseudonana

Declarations

Ethics approval and consent to participate

Not applicable

Consent for publication

Not applicable

Availability of data and materials

All data generated or analyzed during this study are included in this published article and its supplementary information files.

Competing interests

The authors declare no financial interests.

Funding

Financial support from the DFG (FOR2038: Nanopatterned Organic Matrices in Biological Silica Mineralization) is gratefully acknowledged. A.L.P. was supported by the Dutch Research Council (NWO, Grant numbers 718.015.001 to M.B.) This work was also supported the infrastructure project I.Next (Horizon 2020 program of the European Union, Grant # 653706).

Authors' contributions

HLE, FK and ALP performed and analyzed the DNP solid-state NMR experiments. All authors contributed to writing the paper and approved the final manuscript.

References

1. Akiva-Tal A, Kababya S, Balazs YS, Glazer L, Berman A, Sagi A, Schmidt A. In situ molecular NMR picture of bioavailable calcium stabilized as amorphous CaCO 3 biomineral in crayfish gastroliths. *Proceedings of the National Academy of Sciences of the United States of America* 2011, *108* (36), 14763–14768.
2. Koers EJ, Lopez-Deber MP, Weingarth M, Nand D, Hickman DT, Ndao DM, Reis P, Granet A, Pfeifer A, Muhs A, Baldus M. Dynamic Nuclear Polarization NMR Spectroscopy: Revealing Multiple Conformations in Lipid-Anchored Peptide Vaccines. Angewandte Chemie-International Edition. 2013;52(41):10905–8.
3. Jantschke A, Koers E, Mance D, Weingarth M, Brunner E, Baldus M. Insight into the Supramolecular Architecture of Intact Diatom Biosilica from DNP-Supported Solid-State NMR Spectroscopy. Angewandte Chemie-International Edition. 2015;54(50):15069–73.
4. Chakraborty A, Deligey F, Quach J, Mentink-Vigier F, Wang P, Wang T. Biomolecular complex viewed by dynamic nuclear polarization solid-state NMR spectroscopy. *Biochemical Society Transactions* 2020.
5. Kang X, Kirui A, Muszyński A, Widanage MCD, Chen A, Azadi P, Wang P, Mentink-Vigier F, Wang T. Molecular architecture of fungal cell walls revealed by solid-state NMR. *Nature Communications* 2018, *9* (1), 2747.

6. Roehrich A, Drobny G, Solid-State NMR. Studies of Biomineralization Peptides and Proteins. Acc Chem Res. 2013;46(9):2136–44.
7. Wang T, Phyo P, Hong M. Multidimensional solid-state NMR spectroscopy of plant cell walls. Solid State Nucl Magn Reson. 2016;78:56–63.
8. Groger C, Lutz K, Brunner E. NMR studies of biomineralisation. *Progress in Nuclear Magnetic Resonance Spectroscopy* 2009, *54* (1), 54–68.
9. Tesson B, Masse S, Laurent G, Maquet J, Livage J, Martin-Jézéquel V, Coradin T. Contribution of multi-nuclear solid state NMR to the characterization of the Thalassiosira pseudonana diatom cell wall. Anal Bioanal Chem. 2008;390(7):1889–98.
10. Wisser D, Brückner SI, Wisser FM, Althoff-Ospelt G, Getzschmann J, Kaskel S, Brunner E. 1H–13C–29Si triple resonance and REDOR solid-state NMR—A tool to study interactions between biosilica and organic molecules in diatom cell walls. *Solid State Nuclear Magnetic Resonance* 2015, *66–67*, 33–39.
11. Sumper M, Brunner E. Silica Biomineralisation in Diatoms: The Model Organism Thalassiosira pseudonana. *ChemBioChem* **2008**, *9* (8), 1187–1194.
12. Ni QZ, Daviso E, Can TV, Markhasin E, Jawla SK, Swager TM, Temkin RJ, Herzfeld J, Griffin RG. High Frequency Dynamic Nuclear Polarization. Acc Chem Res. 2013;46(9):1933–41.
13. Bajaj VS, Mak-Jurkauskas ML, Belenky M, Herzfeld J, Griffin RG. Functional and shunt states of bacteriorhodopsin resolved by 250 GHz dynamic nuclear polarization–enhanced solid-state NMR. *Proceedings of the National Academy of Sciences* **2009**, *106* (23), 9244–9249.
14. Koers EJ, van der Cruijsen EAW, Rosay M, Weingarth M, Prokofyev A, Sauvee C, Ouari O, van der Zwan J, Pongs O, Tordo P, Maas WE, Baldus M. NMR-based structural biology enhanced by dynamic nuclear polarization at high magnetic field. *Journal of Biomolecular Nmr* 2014, *60* (2–3), 157–168.
15. Reggie L, Lopez JJ, Collinson I, Glaubitz C, Lorch M. Dynamic Nuclear Polarization-Enhanced Solid-State NMR of a C-13-Labeled Signal Peptide Bound to Lipid-Reconstituted Sec Translocon. *Journal of the American Chemical Society* 2011, *133* (47), 19084–19086.
16. Linden AH, Lange S, Franks WT, Akbey U, Specker E, van Rossum B-J, Oschkinat H. Neurotoxin II Bound to Acetylcholine Receptors in Native Membranes Studied by Dynamic Nuclear Polarization NMR. *Journal of the American Chemical Society* 2011, *133* (48), 19266–19269.
17. Pinto C, Mance D, Sinnige T, Daniels M, Weingarth M, Baldus M. Formation of the beta-barrel assembly machinery complex in lipid bilayers as seen by solid-state NMR. *Nature Communications* 2018, *9*.
18. Joedicke L, Mao J, Kuenze G, Reinhart C, Kalavacherla T, Jonker HRA, Richter C, Schwalbe H, Meiler J, Preu J, Michel H, Glaubitz C. The molecular basis of subtype selectivity of human kinin G-protein-coupled receptors. Nat Chem Biol. 2018;14:284.
19. van der Wel PCA, Hu K-N, Lewandowski J, Griffin RG. Dynamic Nuclear Polarization of Amyloidogenic Peptide Nanocrystals: GNNQQNY, a Core Segment of the Yeast Prion Protein Sup35p. J Am Chem Soc. 2006;128(33):10840–6.

20. Frederick KK, Michaelis VK, Corzilius B, Ong T-C, Jacavone AC, Griffin RG, Lindquist S. Sensitivity-Enhanced NMR Reveals Alterations in Protein Structure by Cellular Milieus. *Cell* 2015, *163* (3), 620–628.
21. Kaplan M, Cukkemane A, van Zundert GCP, Narasimhan S, Daniëls M, Mance D, Waksman G, Bonvin AMJJ, Fronzes R, Folkers GE, Baldus M. Probing a cell-embedded megadalton protein complex by DNP-supported solid-state NMR. *Nature Methods* 2015, *12* (7), 649–652.
22. Kaplan M, Narasimhan S, de Heus C, Mance D, van Doorn S, Houben K, Popov-Celeketic D, Damman R, Katrukha EA, Jain P, Geerts WJC, Heck AJR, Folkers GE, Kapitein LC, Lemeer S, Henegouwen P, Baldus M. EGFR Dynamics Change during Activation in Native Membranes as Revealed by NMR. Cell. 2016;167(5):1241–51.
23. Narasimhan S, Scherpe S, Lucini†Paioni A, van†der†Zwan J, Folkers GE, Ovaa H, Baldus M. DNP-Supported Solid-State NMR Spectroscopy of Proteins Inside Mammalian Cells. Angew Chem Int Ed. 2019;58(37):12969–73.
24. Damman R, Lucini Paioni A, Xenaki KT, Beltrán Hernández I, van Bergen en Henegouwen, PMP, Baldus M. Development of in vitro-grown spheroids as a 3D tumor model system for solid-state NMR spectroscopy. *Journal of Biomolecular NMR* 2020.
25. Wang T, Park YB, Caporini MA, Rosay M, Zhong L, Cosgrove DJ, Hong M. Sensitivity-enhanced solid-state NMR detection of expansin's target in plant cell walls. *Proceedings of the National Academy of Sciences* **2013**, *110* (41), 16444–16449.
26. Kolbe F, Ehren HE, Kohrs S, Butscher D, Reiss L, Baldus M, Brunner E, Solid-state NMR spectroscopic studies of 13C,15N,29Si-enriched biosilica from the marine diatom Cyclotella cryptica. *submitted* 2020.
27. Harrison PJ, Waters RE, Taylor FJR. A BROAD SPECTRUM ARTIFICIAL SEA WATER MEDIUM FOR COASTAL AND OPEN OCEAN PHYTOPLANKTON1. *Journal of Phycology* **1980**, *16* (1), 28–35.
28. Spinde K, Pachis K, Antonakaki I, Paasch S, Brunner E, Demadis KD. Influence of Polyamines and Related Macromolecules on Silicic Acid Polycondensation: Relevance to "Soluble Silicon Pools"? *Chemistry of Materials* 2011, *23* (21), 4676–4687.
29. Fung BM, Khitrin AK, Ermolaev K. An Improved Broadband Decoupling Sequence for Liquid Crystals and Solids. J Magn Reson. 2000;142(1):97–101.
30. Baker LA, Daniels M, van der Cruijsen EAW, Folkers GE, Baldus M. Efficient cellular solid-state NMR of membrane proteins by targeted protein labeling. *Journal of Biomolecular Nmr* 2015, *62* (2), 199–208.
31. Baldus M, Petkova AT, Herzfeld J, Griffin RG. Cross polarization in the tilted frame: assignment and spectral simplification in heteronuclear spin systems. Mol Phys. 1998;95(6):1197–207.
32. Sauvee C, Rosay M, Casano G, Aussenac F, Weber RT, Ouari O, Tordo P. Highly Efficient, Water-Soluble Polarizing Agents for Dynamic Nuclear Polarization at High Frequency. Angewandte Chemie-International Edition. 2013;52(41):10858–61.
33. Herth W, Zugenmaier P. Ultrastructure of the chitin fibrils of the centric diatom Cyclotella cryptica. *Journal of Ultrastructure Research* 1977, *61* (2), 230–239.

34. Herth W. The site of β-chitin fibril formation in centric diatoms. II. The chitin-forming cytoplasmic structures. *Journal of Ultrastructure Research* 1979, *68* (1), 16–27.
35. Synytsya A, Novák M. Structural diversity of fungal glucans. Carbohyd Polym. 2013;92(1):792–809.
36. Fontaine T, Simenel C, Dubreucq G, Adam O, Delepierre M, Lemoine J, Vorgias CE, Diaquin M, Latgé J-P. Molecular Organization of the Alkali-insoluble Fraction ofAspergillus fumigatus Cell Wall. J Biol Chem. 2000;275(36):27594–607.
37. Mance D, Weingarth M, Baldus M. Solid-state NMR on complex biomolecules: Methods and applications. In *Modern Magnetic Resonance*, 2018; pp 487–503.
38. Tan KO, Mardini M, Yang C, Ardenkjær-Larsen JH, Griffin RG. Three-spin solid effect and the spin diffusion barrier in amorphous solids. Science Advances. 2019;5(7):eaax2743.
39. Mance D, Gast P, Huber M, Baldus M, Ivanov KL. The magnetic field dependence of cross-effect dynamic nuclear polarization under magic angle spinning. *The Journal of Chemical Physics* 2015, *142* (23), 234201.
40. Corzilius B, Andreas LB, Smith AA, Ni QZ, Griffin RG. Paramagnet induced signal quenching in MAS–DNP experiments in frozen homogeneous solutions. J Magn Reson. 2014;240:113–23.
41. Pawolski D, Heintze C, Mey I, Steinem C, Kröger N. Reconstituting the formation of hierarchically porous silica patterns using diatom biomolecules. *Journal of Structural Biology* 2018, *204* (1), 64–74.
42. Kotzsch A, Pawolski D, Milentyev A, Shevchenko A, Scheffel A, Poulsen N, Shevchenko A, Kröger N. Biochemical Composition and Assembly of Biosilica-associated Insoluble Organic Matrices from the Diatom Thalassiosira pseudonana. *Journal of Biological Chemistry* 2016, *291* (10), 4982–4997.
43. Look GC, Murphy MM, Campbell DA, Gallop MA. Trimethylorthoformate: A mild and effective dehydrating reagent for solution and solid phase imine formation. Tetrahedron Lett. 1995;36(17):2937–40.
44. Huang M-J, Lee KS. 1H and 13C NMR chemical shift assignments of agmatine analogues, (3-aminopropyl)guanidine and (trans-4-aminocyclohexyl)guanidine. Mol Phys. 2005;103(15–16):2229–37.
45. SIETSMA JH, WESSELS JGH. Evidence for Covalent Linkages between Chitin and β-Glucan in a Fungal Wall. *Microbiology* **1979**, *114* (1), 99–108.
46. Bayro MJ, Huber M, Ramachandran R, Davenport TC, Meier BH, Ernst M, Griffin RG. Dipolar truncation in magic-angle spinning NMR recoupling experiments. *The Journal of Chemical Physics* 2009, *130* (11), 114506.
47. Poulsen N, Sumper M, Kröger N, Biosilica formation in diatoms: Characterization of native silaffin-2 and its role in silica morphogenesis. *Proceedings of the National Academy of Sciences* 2003, *100* (21), 12075–12080.
48. Poulsen N, Kröger N. Silica Morphogenesis by Alternative Processing of Silaffins in the Diatom Thalassiosira pseudonana. J Biol Chem. 2004;279(41):42993–9.

Figures

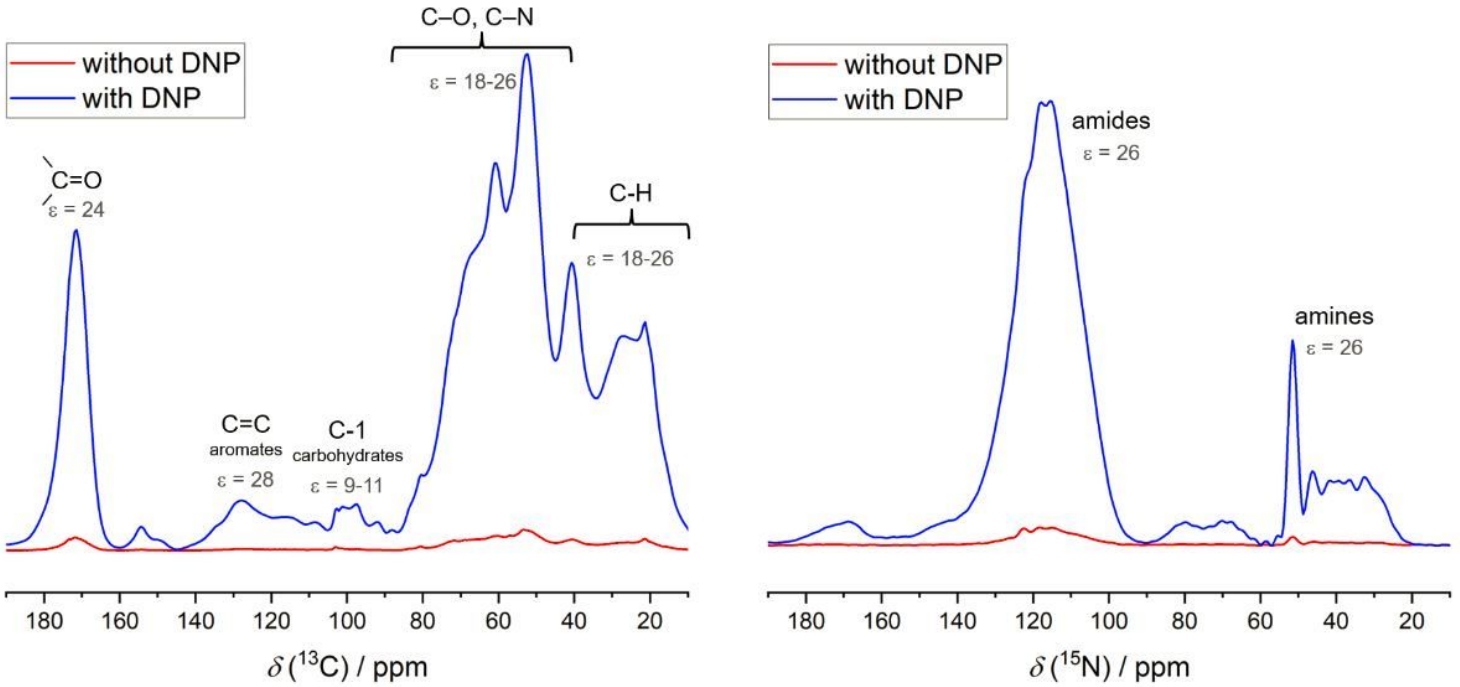

Figure 1

1D CP data of C. cryptica with and without DNP enhancement. Left: The 13C CP spectrum shows DNP enhancement factors ranging from 9 (carbohydrates) to 18-28 for other carbon moieties. Right: In the 15N CP spectrum an enhancement of 26 for both amide and amine signals is observed.

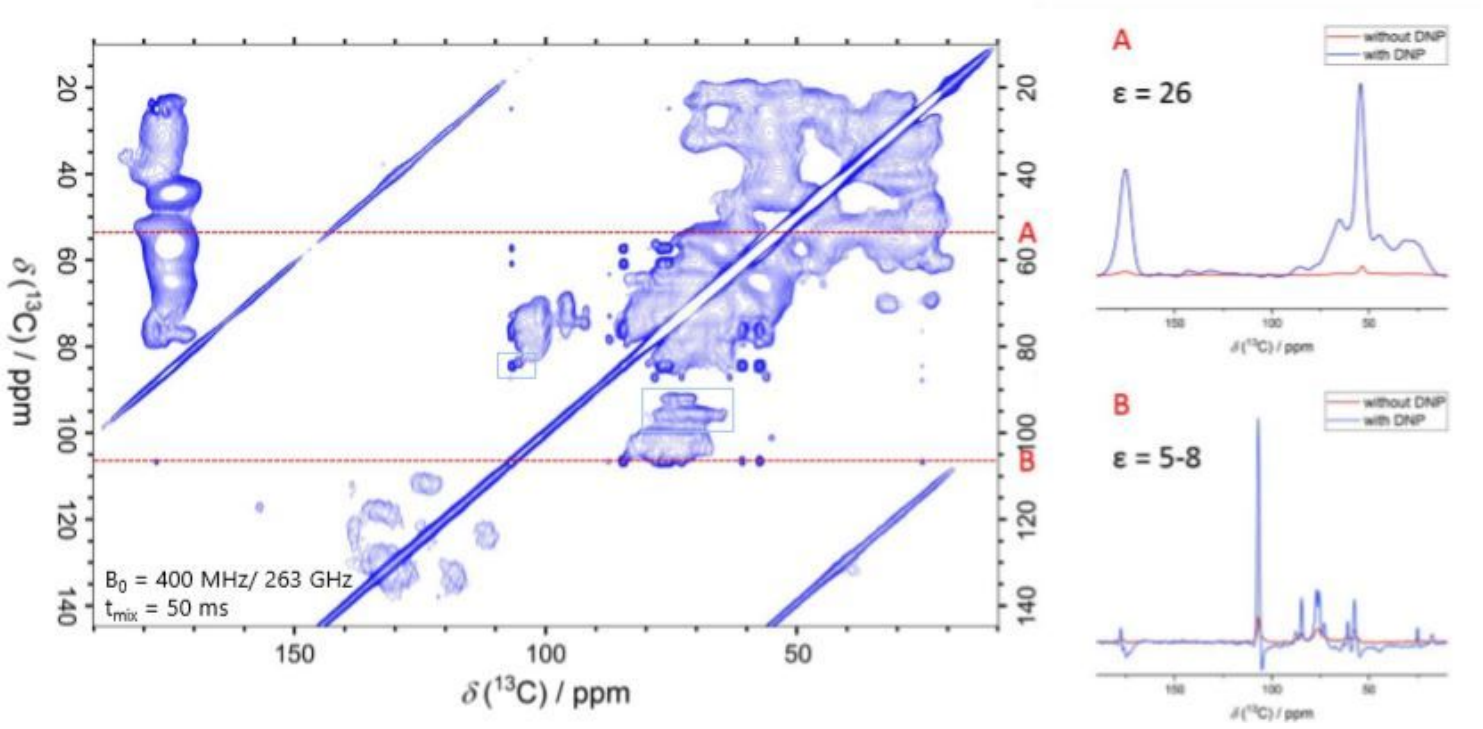

Figure 2

DNP-supported Proton-Driven Spin Diffusion (PDSD) experiment of isotope-enriched C. cryptica biosilica using a mixing time of 50 ms and an MAS rate of 9 kHz. For better resolution, the enhancements were determined from 1D slices in the fingerprint region for protein C-alpha (slice A, 53 ppm, enhancement = 26) and characteristic for carbohydrates (Slice B, 105 ppm, Enhancement = 5-8).

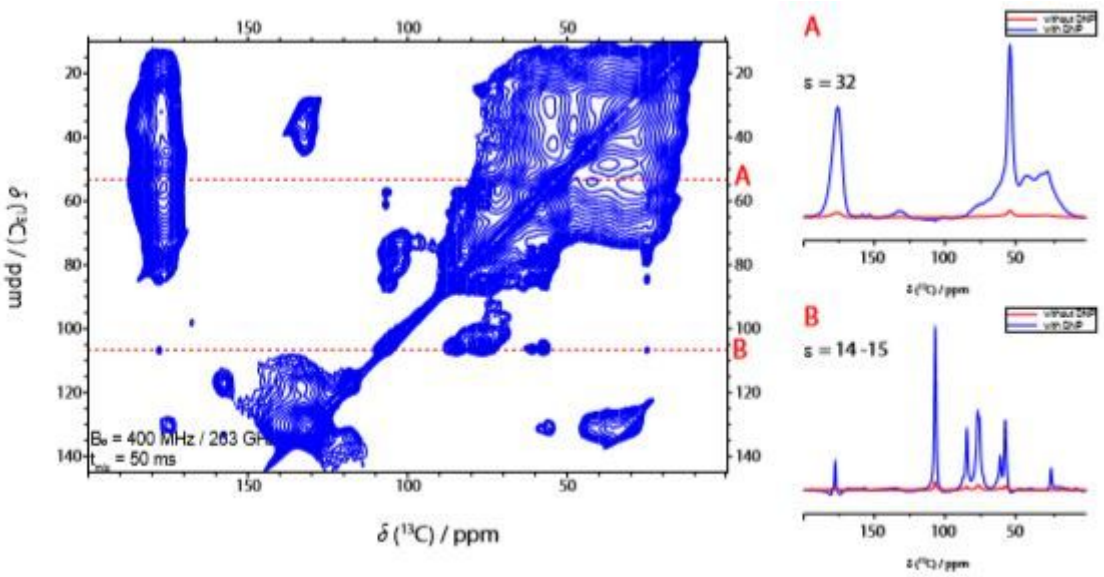

Figure 3

DNP-supported Proton-Driven Spin Diffusion (PDSD) experiment of isotope-enriched T. pseudonana biosilica using a mixing time of 50 ms and a MAS rate of 9 kHz. For better resolution, enhancements were again determined from 1D slices in the fingerprint region for protein C-alpha (slice A, 53 ppm, enhancement = 32) and characteristic for carbohydrates (Slice B, 105 ppm, Enhancement = 14-15).

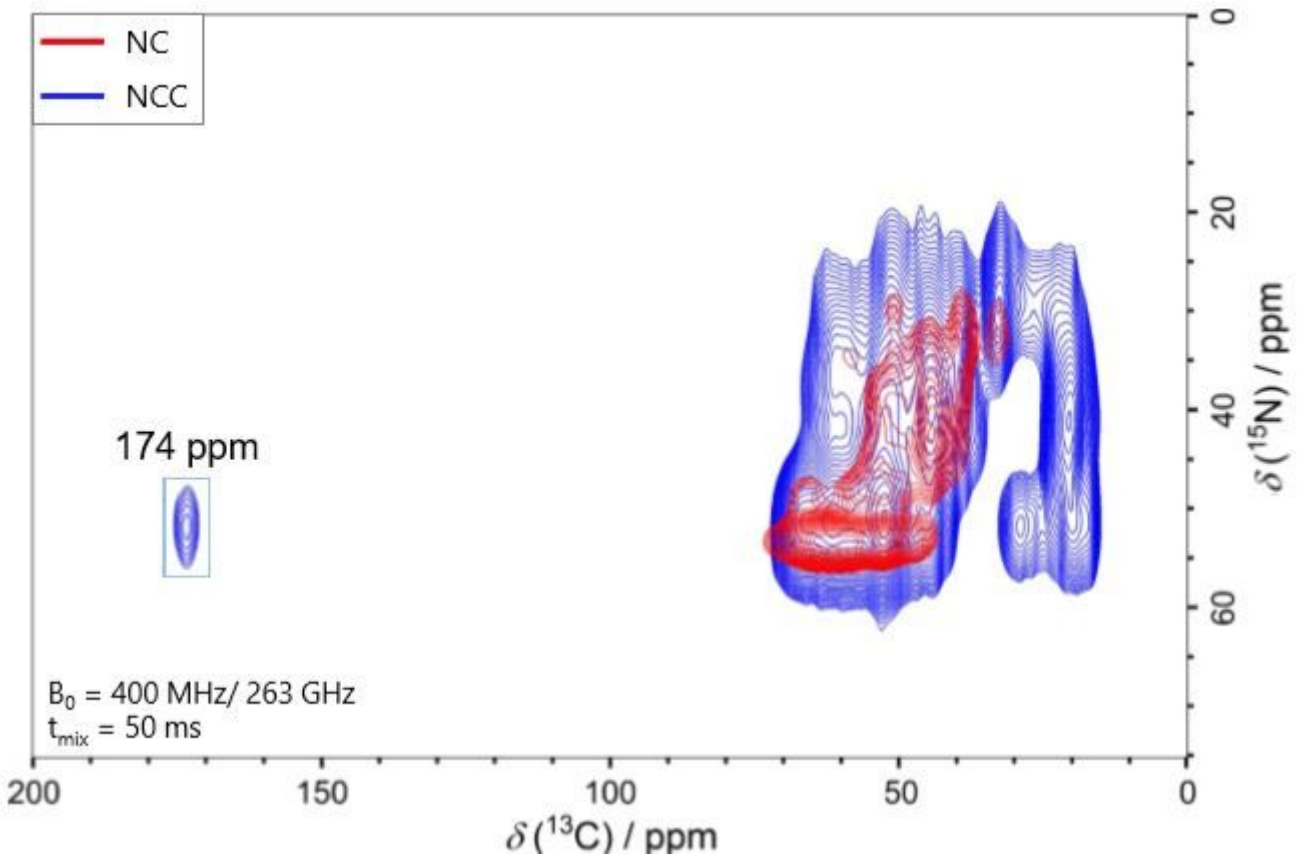

Figure 4

DNP-supported NC and NCC NMR correlation experiments of isotope-enriched C. cryptica biosilica. In both experiments, 15N->13C transfer was established using a SPECIFIC-CP transfer step of 3ms. In the NCC correlation experiment (blue) a mixing time of 50 ms was used for proton-driven spin diffusion (PDSD).

Supplementary Files

This is a list of supplementary files associated with this preprint. Click to download.

- BMRLD2000020neu.pdf
- ehrenetalSI.docx